Molecular determinants of efficient cobalt-substituted hemoprotein production in *E. coli*

Brian R. Weaver[a,*], Lydia J. Perkins[a,*], Froylan Omar Fernandez Candelaria[a], Judith N. Burstyn[a,+], Andrew R. Buller[a,+]

[a]Department of Chemistry, University of Wisconsin–Madison, 1101 University Avenue, Madison, Wisconsin 53706, United States

* = These authors contributed equally

+ = To whom correspondence should be addressed: Andrew R. Buller (arbuller@wisc.edu)

Key Words: *Ferrochelatase, metal homeostasis, multiplexed screening, enzyme kinetics*

ABSTRACT: Exchanging the native iron of heme for other metals yields artificial metalloproteins with new properties for spectroscopic studies and biocatalysis. Recently, we reported a method for biosynthesis and incorporation of a non-natural metallocofactor, cobalt protoporphyrin IX (CoPPIX), into hemoproteins using the common laboratory strain *E. coli* BL21(DE3). This discovery inspired us to explore the determinants of metal specificity for metallocofactor biosynthesis in *E. coli*. Herein we report detailed kinetic analysis of the ferrochelatase responsible for metal insertion, *Ec*HemH. This enzyme exhibits a small, less than two-fold preference for Fe^{2+} over the non-native Co^{2+} substrate *in vitro*. To test how mutation impacts *Ec*HemH, we used a surrogate metal specificity screen to identify variants with altered metal insertion preferences. This engineering process led to a variant with a ~30-fold shift in specificity towards Co^{2+}. When assayed *in vivo*, however, the impact of this mutation is small compared to the effects of altering the external metal concentrations. These data suggest that cobalt incorporation into protoporphyrin IX is enabled by the native promiscuity of *Ec*HemH coupled with BL21's impaired ability to maintain transition metal homeostasis. With this knowledge, we generated a method for CoPPIX production in rich media, which yields cobalt-substituted hemoproteins with >95% cofactor purity and yields comparable to standard expression protocols for the analogous native hemoproteins.

Proteins bearing unnatural metallocofactors are useful tools to study metalloprotein function, expand the reactivity of natural proteins, and catalyze abiological reactions.[1,2] In particular, metal-substituted hemoproteins have been explored extensively because they have unique reactivity,[3–8] may serve as spectroscopic probes,[9–12]and have unique imaging properties. While there are diverse methods to generate proteins loaded with unnatural metalloporphyrin cofactors both *in vivo* and *in vitro*, [3,13–15] many of these strategies require exogenous synthesis of the unnatural metalloporphyrin and rely on low-efficiency methods for inserting the cofactor into the protein. We recently reported a method for the *de novo* biosynthesis of the non-native heme analog, cobalt protoporphyrin IX (CoPPIX), in *E. coli* BL21(DE3) and its incorporation into hemoproteins.[16] This fully biosynthetic method streamlined the production of CoPPIX-bearing artificial metalloproteins and spurred further inquiry into the determinants of metal specificity in metalloporphyrin assembly in *E. coli* BL21(DE3).

Nature typically assembles metalloproteins and metallocofactors with impressive fidelity. Nevertheless, there are reports of improperly metalated heme cofactors occurring in living systems. In humans, zinc protoporphyrin IX (ZnPPIX) is a biomarker for altered iron homeostasis and is implicated in some thalassemias.[17] Majtan et al. found that *E. coli* BL21-Rosetta2(DE3), when passaged for several days through iron-poor, cobalt-rich media, adventitiously biosynthesized and incorporated CoPPIX into both endogenous[18] and heterologously expressed[19] hemoproteins. We reported an expansion of this finding by showing that the standard laboratory strain *E. coli* BL21(DE3) innately possesses the ability to biosynthesize and incorporate CoPPIX, without passaging. Addition of an inexpensive cobalt salt to iron-deficient minimal media was sufficient to produce cobalt substituted hemoproteins from diverse fold families with >95% cobalt loadings. Others similarly found that ZnPPIX can be over-produced by an engineered B-derived strain of *E. coli* under iron-poor, zinc-rich fermentation conditions.[20] These reports indicate that heme biosynthesis in *E. coli* may be manipulated toward production of non-natural metalloporphyrin cofactors. However, these cases of alternative heme metalation in *E. coli* depend on iron-deficient growth

conditions to reduce production of the native heme cofactor. Such conditions severely limit cell growth and, correspondingly, the titers of expressed cobalt substituted hemoproteins are low when compared to standard expression of hemoproteins.[16] We envisioned that by understanding determinants of cofactor metalation specificity, we might develop a more efficient process for synthesis and incorporation of the CoPPIX cofactor.

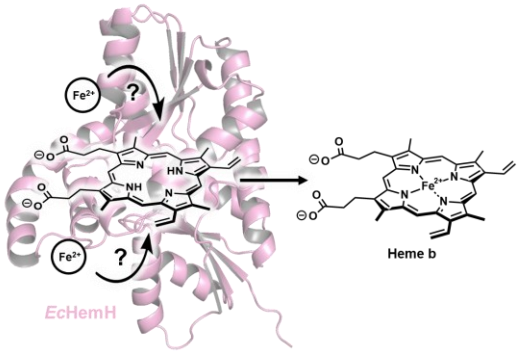

Figure 1. Reaction of *Ec*HemH with ferrous iron and protoporphyrin IX (PPIX) to make heme b. Two distinct molecular pathways for metal insertion have been proposed and the residues responsible for orienting the metal prior to insertion and deprotonation of the pyrrole differ accordingly. The pink cartoon is an AlphaFold model of *Ec*HemH.[21]

Metalation of tetrapyrrole-derived cofactors (heme, siroheme, cobalamin, and others) is a physiologically irreversible process catalyzed by a diverse class of enzymes called chelatases.[22] In *E. coli*, the final step in heme b biosynthesis is incorporation of ferrous iron into protoporphyrin IX (PPIX), catalyzed by PPIX ferrochelatase (*Ec*HemH) (Figure 1A). Eukaryotic HemH homologs, denoted FECH, particularly those from *S. cerevisiae* and *H. sapiens*, are well-studied.[23–25] *Ec*HemH is a membrane-associated enzyme and has been previously expressed and purified,[26,27] but no kinetic characterization of *Ec*HemH, or HemH from any other gram-negative bacteria, has been reported. The location of the productive metal binding site and the face of the porphyrin into which the metal is inserted have been debated in the literature.[25,28] Nevertheless, *in vitro* incorporation of non-native metals by several ferrochelatases (HemH homologs) is well-known.[25,29–32] To date, it is unclear how chelatases tune their activity for different metals and many potential effects may contribute depending on the specific protein and metal in question. Distortion of the porphyrin,[33–35] specificity-determining active site residues,[36,37] differential product inhibition,[38] and exogenous metal delivery[30] are suggested to contribute.

Here, we explore *E. coli* BL21(DE3)'s unusual ability to produce CoPPIX *in vivo*. To better understand the native metal specificity of *Ec*HemH, we used purified enzyme to measure catalytic activity with Fe^{2+}, Co^{2+}, Ni^{2+}, Cu^{2+}, and Zn^{2+}. We next asked whether a more selective cobalt chelatase might enable efficient production and incorporation of CoPPIX in iron-rich growth media. We used a substrate-multiplexed metal specificity to identify a single point mutant (L13R) that has a ~30-fold shift in selectivity for Co^{2+} over Fe^{2+} relative to the parent *Ec*HemH. We analyzed the ability of *Ec*HemH variants to discriminately produce CoPPIX over heme in rich growth media and found that, while variants may produce altered specificity profiles *in vivo*, metabolic factors play the predominant role in determining CoPPIX incorporation into co-expressed hemoproteins. Under sufficiently high cobalt concentrations in rich media and in the absence of a specifically engineered chelatase, BL21(DE3) reproducibly yields greater than 95% cobalt-loaded hemoprotein with titers comparable to typical hemoprotein expressions. Our results provide insight into the mechanism and metal selectivity of *Ec*HemH, inform future engineering efforts for metalloporphryin biosynthesis, and demonstrate a straightforward and scalable route to cobalt-substituted hemoprotein production in rich media.

Results

In vitro assessment of *E. coli* ferrochelatase metal promiscuity

We began our investigation by probing the kinetic mechanism and metal specificity of *Ec*HemH (UniProt accession: A0A140NEM8). This protein contains a *C*-terminal His-tag and was over-expressed in *E. coli* BL21(DE3), followed by purification with nickel affinity chromatography yielding approximately 10 mg *Ec*HemH per L culture. While poly-His tags may interfere with the metal binding properties of some enzymes, such constructs for chelatase homologs have been used previously, without complication.[23,39–41] Sodium cholate was added to the lysis, purification, and storage buffers, as the enzyme has been shown to require detergents for solubility.[27] *Ec*HemH is predicted to be membrane associated due to the presence of a 12-residue segment implicated in membrane association.[42]

Using a simple spectroscopic assay, we investigated the ability of *Ec*HemH to catalyze insertion of Fe^{2+}, Co^{2+}, Ni^{2+}, Zn^{2+}, Cu^{2+}, Mn^{2+}, and Mg^{2+} into PPIX. The catalytic activity of ferrochelatase is well-suited to kinetic analysis by electronic-absorption spectroscopy, as the metalation of PPIX imparts unique spectral shifts to the Soret (~400 nm) and Q bands (~500-600 nm). We detected product formation for all metals tested except for Mn^{2+} and Mg^{2+} (Figure 2A and C, S1). The reactivity profile of *Ec*HemH was in good agreement with reported activity of previously characterized ferrochelatase enzymes.[25] To quantify the native iron chelatase activity of *Ec*HemH, we measured initial rates of

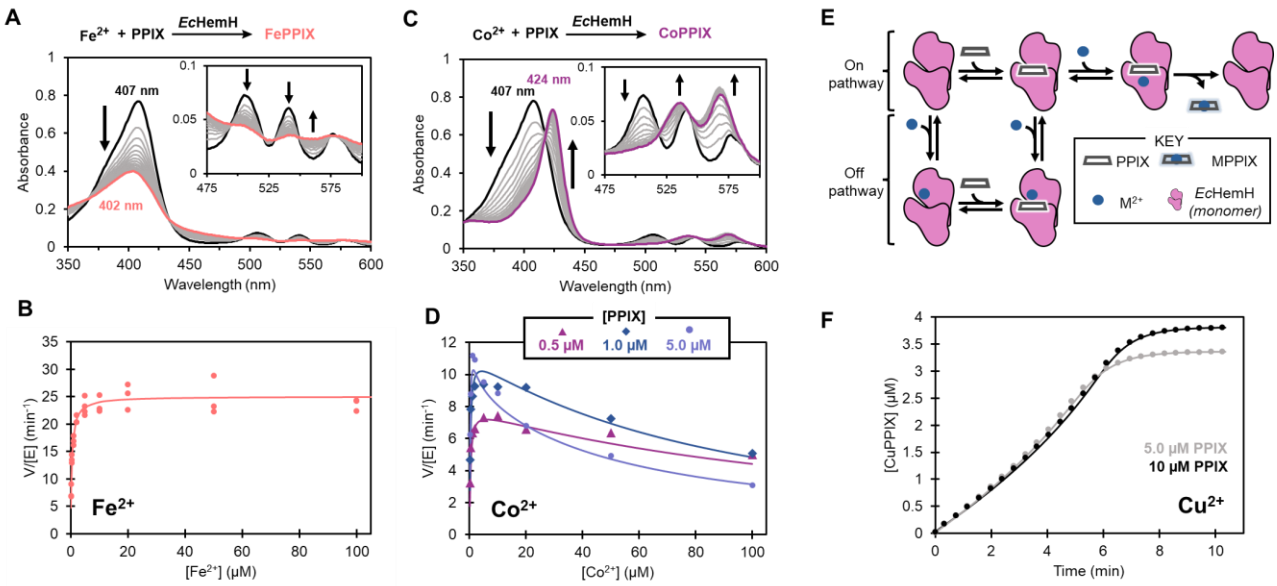

Figure 2. *E. coli* ferrochelatase (*Ec*HemH)-catalyzed insertion of native Fe^{2+} and non-native metals into protoporphyrin IX (PPIX). A) Progress spectra of Fe^{2+} insertion into PPIX by *Ec*HemH. The black trace represents the UV-visible spectrum of 7.5 μM protoporphyrin IX in reaction buffer (100 mM MOPS, 400 mM NaCl, 0.2% w/v Tween 80 at pH 7.0) with 100 nM *Ec*HemH. The metalation reaction was initiated at 25 °C by the addition of 10 μM of Fe^{2+}. To limit competing oxidation to Fe^{3+}, samples were prepared fresh and initial velocities were taken from the first 30 s of data acquisition. Grey lines indicate absorption spectra taken during the reaction progress, and the pink line represents the absorption spectrum of heme b (FePPIX) at the end of the reaction. B) Initial rates of *Ec*HemH-catalyzed heme production plotted as a function of the Fe^{2+} concentration. The concentration of PPIX was 5 μM. These reactions were conducted at 25 °C. The solid line represents the best fit of the data using an ordered sequential binding kinetic model, shown in Figure S2. C) Progress spectra of Co^{2+} insertion into PPIX by *Ec*HemH. The experimental setup is identical to panel A, except that 30 nM *Ec*HemH and 10 μM Co^{2+} were used in the reaction. The purple line represents the absorption spectrum of CoPPIX at the end of the reaction. D) Initial rates of *Ec*HemH-catalyzed CoPPIX production plotted as a function of Co^{2+}. Rates were measured with PPIX concentrations ranging from 0.1-10 μM PPIX, only three concentrations of which are shown here for clarity. The data were fit globally using DynaFit 4. Solid lines represent the best fit of the data using a noncompetitive substrate model (See panel E) and correspond to the kinetic parameters shown in Table 1. Additional data and information about the kinetic model used can be found in Figures S3-S10 of the supplemental information. E) Cartoon representation of proposed noncompetitive substrate inhibition kinetic scheme (See also: Scheme S2). F) Progress curves tracking CuPPIX production over time. Reactions were conducted at 25 °C with approximately 5 μM (grey) or 10 μM (black) PPIX and 100 nM *Ec*HemH and were initiated by the addition of approximately 3.8 μM Cu^{2+}. Solid lines represent the best global fit of the data by DynaFit 4 to the noncompetitive substrate inhibition model (Scheme S2) and correspond the kinetic parameters shown in Table 1.

heme formation spectrophotometrically with variable PPIX and Fe^{2+} concentrations at room temperature (Figure 1B and S2). We fit these data to an ordered sequential mechanism where PPIX binds first, followed by Fe^{2+} binding, as described by Scheme S1. An equilibrium random-ordered mechanism can also describe these data, which results in identical macroscopic constants as the ordered sequential kinetic model.[43] The resulting fit yielded a k_{cat} of 30 min^{-1}, K_M^{Fe} of 0.48 μM Fe^{2+}, and K_M^{PPIX} of 1.1 μM PPIX (Table S7). These values compare favorably with previously characterized ferrocheletase enzymes (Table S3).[32]

We next sought to test the kinetics of CoPPIX formation by *Ec*HemH. We first measured initial rates of CoPPIX production at 5 μM PPIX while varying the Co^{2+} concentration. In contrast to the behavior observed with Fe^{2+}, we observed a decrease in the rate of CoPPIX production with high concentrations of Co^{2+} (Figure 2D). This substrate inhibition has been observed previously with yeast[36] and mouse[35] FECH enzymes, as well as with coproporphyrin (III) ferrochelatase (CpfC) of other species.[40,41] To characterize this inhibition further, we measured initial rates of CoPPIX production while varying the concentrations of both Co^{2+} and PPIX (Figure 2D, 3 of 6 PPIX concentrations shown for clarity). The resulting data show that increasing concentrations of PPIX exacerbate the inhibitory effect of Co^{2+}. These data mirror observations by Davidson, et al. in studies of human HemH with a PPIX analog, mesoporphyrin IX, and Zn^{2+}.[30]

To better understand the nature of Co^{2+} inhibition, we turned to global analysis of the Co^{2+} initial rate data to identify the simplest kinetic mechanism that recapitulates this complex kinetic behavior. A complete accounting of each kinetic model that we tested is provided in the supporting information (Figures S3-S10). Notably, none of the existing kinetic models for chelatases in the literature fit the data.[30,32] On the basis of this analysis, we propose an *Ec*HemH kinetic mechanism that includes two kinetically distinct metal binding modes, only one of which is kinetically productive (Figure 2E). The productive pathway is initiated by PPIX binding. Co^{2+} can then bind in either a

productive mode, leading to metal insertion, or a non-productive mode corresponding to noncompetitive inhibition. In this model, metal can also bind prior to PPIX, but leads to an inhibitory ternary complex. Together, these model features accurately recapitulate key kinetic observations. At low Co^{2+} concentrations, metal binding in the catalytically productive mode (i.e. after PPIX binding) dominates, and the initial velocities increase as the concentration of PPIX increases. However, at high PPIX concentrations, increasing Co^{2+} concentrations slow the metalation because noncompetitive binding is occurs, leading to pronounced substrate inhibition (Figure 2E). We note that Fe^{2+} insertion does not show substrate inhibition within the range of concentrations tested here, nor has substrate inhibition with Fe^{2+} been observed with other ferrochelatases. However, substrate inhibition was previously observed for the Cu^{2+} insertion into PPIX by the yeast homolog. [32] These studies showed a distinctive 'S' shaped progress curves wherein reactions accelerate during a time course due to relief of substrate inhibition. We tracked CuPPIX formation by *Ec*HemH spectroscopically with three different PPIX and Cu^{2+} concentrations and observed the same S-shape in the progress curves (Figure 2F). We fit these progress curve data to the noncompetitive binding model (Figure 2E), and found that the data were well recapitulated, including the characteristic *S*-feature. We compared the macroscopic kinetic parameters for insertion of Fe^{2+}, Co^{2+}, and Cu^{2+}, which affirm the remarkable promiscuity of the enzyme (Table 1).

Table 1. Kinetic profile for *Ec*HemH activity with various metals.

Macroscopic kinetic parameters			
Substrate	k_{cat} (min^{-1})	K_M (metal) (μM)	k_{cat}/K_M (μM^{-1} min^{-1})
Fe^{2+}	30	0.48	63
Co^{2+}	54	1.1	48
Cu^{2+}	34	0.94	36

Highest observed rates for metal insertion			
Substrate	V_0 / [E] (min^{-1})	[PPIX] (μM)	[M^{2+}] (μM)
Fe^{2+}	29	5	10
Co^{2+}	11	5	1
Ni^{2+}	6.8	2	200
Zn^{2+}	17	5	0.5

Apparent macroscopic kinetic parameters for Fe^{2+}, Co^{2+}, and Cu^{2+} are derived from fitting the data to the appropriate kinetic model. Parameters were not well determined for Zn^{2+} or Ni^{2+}. Instead, the highest observed initial rate is given for these metals, along with the corresponding metal and protoporphyrin IX (PPIX) concentrations.

We additionally tested *Ec*HemH activity with Ni^{2+} and Zn^{2+}. We measured initial rates of NiPPIX production at multiple concentrations of PPIX and Ni^{2+}. Like Co^{2+}, these data showed substrate inhibition by the metal that became more pronounced as a function of PPIX (Figure S9). While the proposed mechanism fit these data well, the model was underdetermined, and macroscopic rate constants could not be confidently assigned. Analysis of ZnPPIX formation also showed distinctive kinetic behaviors. These data showed the fastest initial velocity of metal insertion among the various metals tested, but also the strongest substrate inhibition. These features were recapitulated by the noncompetitive substrate inhibition model, but the model was again underdetermined (Figure S8). We cannot rule out other kinetic possibilities for Ni^{2+} or Zn^{2+} based on these data alone and it is possible that different metals engage in distinct kinetic mechanisms. Nevertheless, a heuristic comparison of activity on the various metals highlights the prevalence of substrate inhibition with non-native metals and the relative efficiency of *Ec*HemH with diversity of transition metals.

Bioinformatic analysis of *Ec*HemH sequence and structure

We hypothesized that the promiscuous *Ec*HemH activity with Co^{2+} was the dominant factor in enabling CoPPIX production in BL21(DE3). If true, selective CoPPIX production in iron-rich media might be enabled by altering the specificity of the chelatase via protein engineering to favor Co^{2+} over Fe^{2+}. The structural underpinnings of metal specificity in ferrochelatase homologs are not well understood, although examples of variants with altered specificity have been found.[31]

We used a model generated with AlphaFold to compare structural features of *Ec*HemH to other, structurally characterized homologs (Figure 3A).[21,42] Alignment of *Ec*HemH with the PPIX-bound *Hs*FECH structure (PDB ID: 2HRE, 27% sequence identity) suggested how *Ec*HemH might interact with the porphyrin substrate. The main structural difference between *Hs*FECH and *Ec*HemH is the presence of an iron-sulfur cluster at the *C*-terminus of *Hs*FECH. Despite the low overall sequence identity, many active site residues appear highly conserved. Distinctive residues in *Ec*HemH are Leu13, Phe31, and Cys273, which correspond to Met76, Leu92, and His341 in *Hs*FECH, respectively (Figure 3B). The differences at Leu13 (*E. coli*) and Met76 (human) are noteworthy because these residues lie directly below the porphyrin substrate and Met76 has been implicated in metal specificity for *Hs*FECH.[36,42]

To gain further insight into sequence conservation across the enzyme family, we generated a sequence alignment of 5,026 HemH homologs and visualized active site conservation with logo plots, shown in Figures S11-S20.[44] Several striking patterns were observed. For example, His194, Trp242, Phe269, and Glu275 (*E. coli* numbering) are >99% conserved, suggesting that these residues are especially important for ferrochelatase function. Additionally, the positions corresponding to Leu13 and Phe31 are almost exclusively occupied by hydrophobic residues. This analysis provides evolutionary context for choosing which residues might be most amendable to mutation. We screened site saturation mutagenesis (SSM) libraries at 10 active site residues (Figure 3A, labelled residues). Based on our structural model, we hypothesized these residues might impart changes in metal specificity either by altering metal chelation or by altering the extent and nature of the porphyrin distortion.

Altering metal specificity of *Ec*HemH through site-saturation mutagenesis

Substrate specificity can be a challenging feature to optimize through engineering because traditional approaches typically monitor activity on a single, model substrate as a proxy for overall enzyme performance.[31,45–47]

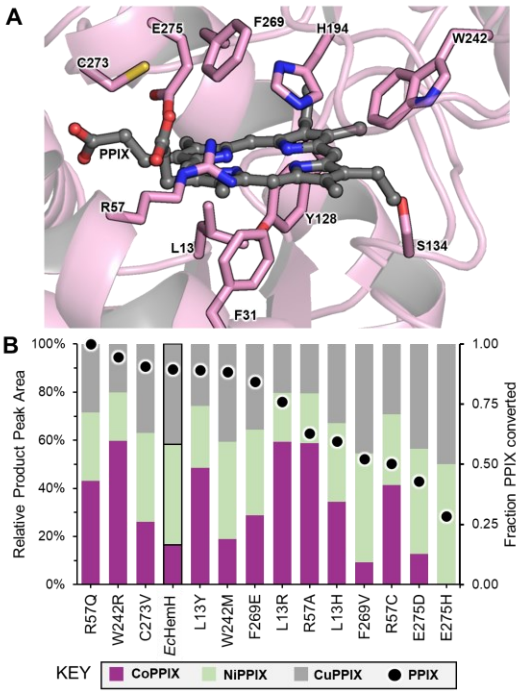

Figure 3. Structural model of *E. coli* ferrochelatase (*EcHemH*) and selection of residues for site saturation mutagenesis. A) AlphaFold active site model of *Ec*HemH (pink) superimposed with PPIX (grey sticks) from PDB 2HRE. B) Results from re-screen of "hits" from site-saturation mutagenesis of *Ec*HemH in cell lysates. Each variant was screened in biological quadruplicate with 10 μM PPIX and a total of 1 mM divalent metal substrate. The resulting porphyrin distribution was analyzed by UPLC. Bars represent the average relative product peak areas corresponding to CoPPIX (purple), NiPPIX (green), and CuPPIX (grey). Black dots represent the relative amount of PPIX substrate remaining, a measure of each variant's total activity. Parent *Ec*HemH is indicated by black borders.

These assays cannot distinguish between enzymes that have higher expression or higher catalytic activity. For the study here, we were more interested in the relative activity of variants on different metals in competition than in the overall catalytic prowess. Therefore, we developed a substrate-multiplexed screen (SUMS) with a mixture of metal ions, which provided direct information on enzyme specificity in a single experiment. The SUMS approach, as applied to protein engineering, has been shown to facilitate discovery of enzyme variants with altered specificity and identification of distal residues that impact catalysis.[48–50]

While relative activity of Fe^{2+} versus Co^{2+} was our principal interest, we found that the specificity between these two metals was exceedingly difficult to monitor in cell lysates. At least two factors confounded analysis. First, Fe^{2+} quickly oxidizes in lysate to Fe^{3+}, which is not a substrate for *Ec*HemH.[32] Second, heme b is catabolized in cell lysate, leading to inconsistent ratios relative to CoPPIX. To work around these challenges, we hypothesized that screening on a mixture of non-native metals would reveal residues that provide the most significant changes to metal specificity relative to the parent. These mutations could subsequently be analyzed to gain insight into their Fe^{2+} specificity using an alternative screening method.

Cell lysates containing *Ec*HemH variants were added to a mixture of Co^{2+}, Ni^{2+}, and Cu^{2+} at relatively high concentration (1 mM total M^{2+}) in the presence of 10 μM PPIX. The relative distribution of the porphyrin products was directly measured using ultra-pressure liquid chromatography (UPLC) and the concentration of each metal was adjusted such that the parent *Ec*HemH produced approximately equal signal for CoPPIX, NiPPIX, and CuPPIX (See supporting information). The resulting data from screening 10 site-saturation mutagenesis libraries are compiled in the supplemental information (Figures S11-S20). We note that the uncertainties associated with screening preclude quantitative analysis on the absolute abundance of each product.

While site-saturation studies of HemH homologs have not been previously reported, the data here were in good general agreement with the detailed analysis performed on point mutants of homologous enzymes. For example, the *Ec*HemH H194X library yielded no active variants (Figure S10). Studies of corresponding variants of FECH (H263C and H263A *Hs*FECH and H235L *Sc*FECH) indicated these variants were inactive or had only trace activity.[24,51,52] Indeed, H194 is nearly 100% conserved among HemH/FECH homologs, consistent with an essential catalytic role.

To directly compare specificity shifts among variants from different libraries, we re-screened in parallel a subset of variants that showed the largest shifts in specificity in the initial screen. While the trends in activity were generally reproducible, several variants had different specificities in this follow-up assessment when compared to the initial screens (e.g. L13R, compare Figure 3 to Figure S11). From the re-screen data, we identified several variants with altered metal specificity compared to the parent *Ec*HemH that we chose for further validation in comparison against Fe^{2+} (Figure 3B).

Assessing *Ec*HemH variant specificity for Fe^{2+} versus Co^{2+}

We next sought to investigate how variants with *in vitro* changes in metal specificity altered metalloporphyrin incorporation into hemoproteins *in vivo.* Cells harboring over-expressed *Ec*HemH variants were grown in rich media supplemented with a 4:1 ratio of exogenous Co^{2+} to Fe^{2+}, such that the bioavailable metal pool was consistent and well-defined. To directly assess the effect of chelatase identity on hemoprotein loading, we co-expressed *Ec*HemH with the hemoprotein, dye-decolorizing peroxidase (DyP, UniProt Accession E3G9I4). DyP binds free PPIX, CoPPIX, and heme b promiscuously.[53] Following

expression, DyP was purified by nickel-affinity chromatography and the relative Co^{2+} and Fe^{2+} content of the protein samples was measured using inductively coupled plasma mass spectrometry (ICP-MS). This analysis showed several variants incorporated more CoPPIX relative to the parent *Ec*HemH, including L13R, L13H, R57Q, and E275D (Figure 4A, S21). Many factors, such as enzyme expression level, may impact metalation outcomes. Indeed, these *in*

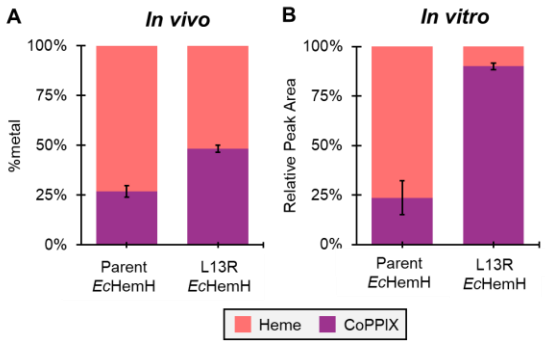

Figure 4. Competition experiments for Co^{2+} and Fe^{2+} incorporation into protoporphyrin IX (PPIX) by parent *Ec*HemH and L13R *Ec*HemH variant. A) Distribution of MPPIX products obtained from co-expression of parent and L13R *Ec*HemH with dye-decolorizing peroxidase (DyP) with a defined mixture of 50 μM Fe^{2+} and 100 μM Co^{2+} added to the growth media. DyP was purified by Ni-affinity chromatography and digested in nitric acid prior to analysis by ICP-MS. Data are average of triplicate ICP-MS measurements. B) *In vitro* measurement of Co^{2+} versus Fe^{2+} incorporation into PPIX by purified parent and L13R *Ec*HemH enzymes. Reactions were conducted in 100 mM Tris-HCl buffer with 400 mM NaCl and 0.2% Tween 80. The concentration of enzyme added was 250 nM and the concentration of PPIX was 5.0 μM. Reactions were initiated with the addition of 50 μM each of Fe^{2+} and Co^{2+} in 0.5 mM ascorbate. After 20 minutes, reactions were quenched with acid and extracted into organic solvent. The relative concentrations of porphyrin products were analyzed by UPLC using the absorbance at 400 nm (FePPIX and PPIX) and 423 nm (CoPPIX). Error bars represent the standard deviation of quadruplicate UPLC measurements.

vivo experiments relied on overexpression of *Ec*HemH and its variants to circumvent the native *Ec*HemH regulation[54–56] and deliver high concentrations of enzyme. However, there remained the possibility that high titers of *Ec*HemH may influence metalloporphyrin production relative to the native BL21(DE3) system that motivated this study. We therefore expressed and purified DyP without overexpressing *Ec*HemH and assessed its metal content. This experiment was intended as a negative control, but instead showed that the CoPPIX content of DyP *without* overexpression of *Ec*HemH was the same or higher than any other conditions tested (Figure S21). This result was the first clue that, to our surprise, ferrochelatase specificity may be a minor contributor to *in vivo* metalation outcomes. To rigorously test this new hypothesis, we validated a single variant with altered specificity and explored its impact (or lack thereof) on *in vivo* PPIX metalation.

Testing the effects of altered chelatase specificity

We selected *Ec*HemH L13R to assess the change in metal specificity relative to parent. Rather than determine complex kinetic parameters with this enzyme, we opted for a direct measurement of the change in selectivity by assaying the metalation outcome when Co^{2+} and Fe^{2+} are in direct competition. Excess ascorbate was added to maintain the ferrous oxidation state and product formation was analyzed by UPLC. This analysis revealed that the L13R mutation imparts a ~30-fold shift in selectivity for Co^{2+} relative to parent under these conditions (Figure 4B).

We next asked whether co-expression of the cobalt selective *Ec*HemH variant L13R had any significant impact on CoPPIX versus heme incorporation in rich media. We compared the effect of co-expression of parent *Ec*HemH versus the L13R variant with DyP at substantially higher concentrations of cobalt (500 μM) in rich media without added iron. We further compared these conditions to DyP expressed in 'regular' BL21(DE3), that only contains natively expressed *Ec*HemH. To our surprise, the resulting DyP hemoprotein samples contained greater than 95% CoPPIX in all cases, even the intended negative control with no co-expression of a ferrochelatase (Figure 5A). These results refuted our initial hypothesis that alterations to chelatase specificity would lead to more efficient CoPPIX incorporation into hemoproteins *in vivo*. Instead, we re-investigated metabolic factors that may contribute to CoPPIX accumulation.

Effect of cobalt concentration, *E. coli* strain, and metal identity on metalloporphyrin production

We studied the influence of cobalt concentration in rich media (Terrific Broth) on the metalloporphyrin content of expressed hemoprotein. We were delighted to see that addition of 1 mM of Co^{2+} yielded >90% cobalt incorporation in rich media (Figure 5B). Although the wet cell mass derived from these expressions decreased as more cobalt was added, the holoprotein titers per liter cell culture were only slightly diminished (Table S4). Based on our earlier observations in minimal media,[16] we hypothesized that the cytotoxic effect of high intracellular cobalt concentrations may be mitigated by the expression of a hemoprotein, which serves as a sink for excess, toxic Co^{2+} and CoPPIX.

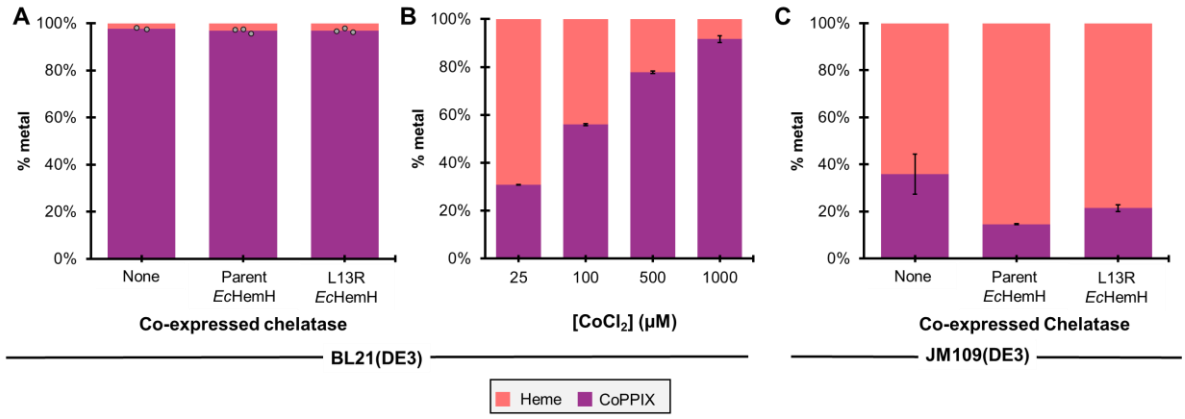

Figure 5: Effect of HemH expression, cobalt concentration, and *E. coli* expression strain on the distribution of CoPPIX- and heme-loaded DyP A) Metal content analysis of DyP by ICP-MS. Proteins were expressed in BL21(DE3) in the absence of a co-expression vector, with parent *Ec*HemH, and with *Ec*HemH L13R. $CoCl_2$ (1 mM) and 250 μM δ-aminolaevulinic acid were added at the time of induction. Dots represent biological replicates. B) ICP-MS measurements of DyP expressed in BL21(DE3) with various amounts of cobalt. Cobalt was added when OD_{600} reached 0.2–0.3, prior to induction with d-arabinose. Measurements were made in triplicates and error bars represent standard deviation. C) ICP-MS measurements of DyP expressed in JM109(DE3) with parent and L13R *Ec*HemH co-expression, and in the absence of chelatase co-expression. Expression conditions were identical to that of Figure 6A. Measurements were made in triplicate and error bars represent standard deviations.

We next tested whether CoPPIX production ability was unique to BL21(DE3). We carried out expression experiments with JM109(DE3), a K12-derived strain whose metal homeostasis is well-studied.[57] Overall, CoPPIX production was markedly less efficient in this strain, yielding less than 40% Co incorporation under the same expression conditions (Figure 5C). Overexpression of *Ec*HemH decreased CoPPIX production, suggesting that the dynamics of porphyrin metabolism may be affected by HemH overexpression. Satisfyingly, L13R HemH co-expression did yield improved CoPPIX relative to the parent *Ec*HemH, although the effect was modest in this strain and heme b was still the major cofactor bound.

The surprisingly efficient incorporation of cobalt into PPIX by BL21(DE3) described here inspired us to test the same method for the incorporation of other metals: copper, nickel, and zinc. Analogous to expression with cobalt, 1 mM of $CuCl_2$, $NiCl_2$, and $ZnCl_2$ were added to 1 L of culture expressing DyP in TB media at the time of induction. DyP was purified and the metalloporphyrin content interrogated by UPLC (Figure S22). Zinc and copper supplemented cultures appeared to contain exclusively the native heme cofactor and unmetallated PPIX. The DyP resulting from expression with added nickel contained mostly heme and unmetallated PPIX, but also a small amount of NiPPIX. As the proportion of NiPPIX bound is relatively low, we did not pursue this potential cofactor further and instead returned to CoPPIX, which was the principal focus of the present study.

Validation of a method for cobalt-substituted hemoproteins in rich media

With this new perspective on the determinants of CoPPIX production, we set out to generate a robust method for production of cobalt substituted hemoprotein in rich media. We found that the timing of addition of 1 mM Co^{2+} to the media had no significant effect on the metalloporphyrin content and yield of holoprotein (Table S5). Consequently, we converged on a protocol where metal is added at the time of induction, along with δALA, which was convenient and effective. With this method we were able to obtain CoDyP at titer of 43 mg protein per L cell culture, and the resulting proteins were >95% cobalt loaded relative to iron. This yield represents a nearly 10-fold improvement in protein titer over our previous method in minimal media,[16] gives similar titers to expression of the native heme-loaded protein (Figure 6).

Lastly, we tested the efficiency of cobalt-substituted hemoprotein production with a different protein scaffold, the P450 enzyme CYP119 from *S. acidcaldarous* under pET22b (IPTG-inducible) and pBAD (arabinose-inducible) expression systems. From 1 L of cell cultures in rich media we obtained 2 mg and 43 mg of ~95% CoPPIX loaded hemoprotein from the pET22b and pBAD systems, respectively. This expression compares favorably with that of the analogous heme proteins, which, in our hands, were obtained at 3 mg and 40 mg per L culture. Furthermore, this method requires virtually no additional steps or genetic manipulations relative to that of canonical heme protein, aside from the addition of an inexpensive cobalt salt ($CoCl_2$) at the time of induction.

Discussion

We performed steady-state kinetic characterization of *Ec*HemH with a variety of metals and found that that this enzyme has a notable substrate inhibition with Co^{2+}. One molecular interpretation consistent with this phenomenon is metal ion binding at two different sites, which has

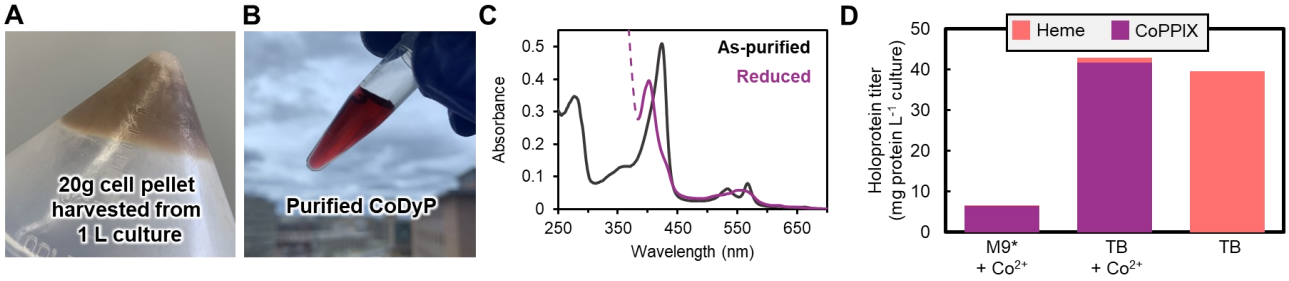

Figure 6. Heterologous expression and purification of cobalt substituted DyP from *E. lignoliticus* in rich media. A) Cell pellet derived from a 1 L culture expression of DyP supplemented with 1 mM $CoCl_2$. B) Sample of purified CoDyP. C) UV-visible spectra of as-purified CoDyP and after reduction with sodium dithionite (magenta). D) Expression titers for Co and native DyP in different growth media M9* is a modified minimal media, and TB is terrific broth.

been proposed for other ferrocheletases.[25] In this kinetic model (Figure 2E), the binding mode that is populated when no PPIX is present is kinetically off-pathway and inhibitory. Structural analysis of the *S. cerevisiae* (PDB 1L8X) and *B. subtilis* (PDB 3M4Z) chelatases observed metal ion binding to Glu275 and His194 (*E. coli* numbering) in the absence of porphyrin.

We hypothesize that these two residues may comprise the inhibitory binding site, which sits 'on top' of the porphyrin when the hydrophobic binding interface is oriented 'below' (Figure S23). This combination of kinetic and structural evidence suggests that metalation occurs from the bottom face of the porphyrin, as has been proposed for the human FECH enzyme.[36] This region of the protein contains Leu13, where we found that mutation strongly influenced metal specificity. In this scenario, the metal is desolvated as it binds to the PPIX pyrrole nitrogens in the hydrophobic enzyme environment. A base is required to deprotonate two pyrrole rings and steric considerations demand that these protons are removed from the opposite face of from which metal insertion occurs.[58] In *Ec*HemH, His194 is positioned to play the role of general base, a hypothesis corroborated by the absence of any chelatase activity in the H194X site saturation mutagenesis library.

Our initial hypothesis was that a low level of chelatase promiscuity was the main enabler of adventitious CoPPIX production in BL21(DE3). Noncompetitive substrate inhibition decreases the overall rate of enzyme catalysis when two metals are placed in competition but does otherwise affect the distribution of products. This inhibition notwithstanding, activity on Fe^{2+} and Co^{2+} was generally similar, indicating that *Ec*HemH is an effective cobalt chelatase. To test the effect of chelatase metal specificity on the production of CoPPIX versus heme in BL21(DE3), we undertook an engineering campaign to improve the Co^{2+} selectivity of the native BL21(DE3) ferrochelatase. The enzyme was surprisingly tolerant to mutation, as site saturation mutagenesis at seven of 10 active site residues yielded active chelatase variants. By screening on a mixture of metal substrates, we were able to probe the influence of residues on metal selectivity in a fashion that is decoupled from overall protein activity. Mutations throughout the active site have marked effects on metal specificity indicating that complex and synergistic interactions with PPIX, metal, and active site residues all influence metal insertion. These observations align with previous studies that link porphyrin distortions in the active site to metal specificity.[33] We identified a mutation, L13R, that causes a 30-fold shift in specificity toward cobalt insertion. The discovery of this variant enabled us to explore how expression of this cobalt-favored chelatase affected the distribution of MPPIX products generated *in vivo*.

Notably—and contrary to our initial hypothesis—we found that the metal specificity of an over-expressed chelatase plays only a minor role in determining the distribution of metalated porphyrins in BL21(DE3). Large changes in Co^{2+} versus Fe^{2+} specificity, such as those exhibited by the variant L13R, do not outweigh the myriad other metabolic factors governing PPIX metalation. Indeed, we found that the native promiscuity of *Ec*HemH is already sufficient for efficient CoPPIX production *in vivo*.

Metal homeostasis is a key factor in determining the distribution of metalated porphyrin products in *E. coli*. BL21-derived strains have been shown to lack the entirety of the *rcn* operon,[57,59] which is responsible for Co^{2+} and Ni^{2+} efflux.[60,61] We hypothesize that the success of this cobalt-substituted hemoprotein expression method is dominated by the inability of *E. coli* BL21(DE3) to efflux cobalt. Instead, a high concentration of cobalt in the growth media leads to high cytosolic cobalt concentrations and, as a result, efficient production of CoPPIX by the natively promiscuous chelatase. Consistent with this hypothesis, the K12-derived strain JM109(DE3), which contains a functional *rcn* operon, was far less effective than BL21(DE3) at production of CoPPIX. However, there are many additional differences between BL21 and K12-derived strains of *E. coli*, including changes in central carbon metabolism.[62] There may be additional differences in CoPPIX breakdown that influence how much of the cofactor is accumulated in different strains. Further studies will be required to elucidate the interplay between these diverse factors. For example, in pathogenic *E. coli*, heme is degraded by the heme oxygenase, ChuS (UniProt accession: A0A271QSA5), which is not present in BL21-derived strains.[63,64] These enzymes catalyze oxidative ring opening of the iron porphyrin cofactor, yielding the linear tetrapyrrole, biliverdin Ixα. These transformations proceed through an iron-oxo intermediate and are inhibited by non-native metalloporphyrins, such as CoPPIX.[65,66] Heme catabolism in non-pathogenic *E. coli,* such as BL21, is not as well

understood.[67,68] It is possible that *E. coli* BL21(DE3) harbors a yet uncharacterized heme-degrading enzyme, or that our and others' observations of heme loss in cell lysates are due to an alternative, non-enzymatic process. Regardless, native heme catabolic pathways may be specific to heme, allowing CoPPIX to accumulate under expression conditions while excess heme is quickly degraded.

Conclusions

Hemoproteins comprise a diverse family of widely studied and used biocatalysts. Often, BL21(DE3) *E. coli* is the organism used to produce these hemoproteins—and the cofactors they bear—at high titers. By studying the metalation and incorporation of a non-native heme analog, CoPPIX, we provide insight into how biological metalation is controlled in this ubiquitous model organism, and guide future campaigns to engineer metallocofactor biosynthesis. Metalloporphyrin distribution may be sensitive to many factors including chelatase specificity, environmental metal concentrations, metal homeostasis machinery, and cofactor catabolism. In nature, these factors work in concert to ensure proper metalation of heme. In contrast, laboratory expression conditions can redirect this machinery towards efficient biosynthesis of CoPPIX. We hypothesize this process proceeds according to the following paradigm: *E. coli* BL21(DE3) does not contain the otherwise common *rcn* operon for efflux of transition metals. These cells grow as normal in rich media and quickly scavenge all available Fe^{2+}, much of which is used by *Ec*HemH to produce heme and support cellular respiration. Once cultures are grown to mid-log phase and a high concentration of cobalt is added, the cobalt is imported and accumulates intracellularly. Consequently, there is a large bioavailable pool of Co^{2+} with minimal Fe^{2+} remaining. The native chelatase, *Ec*HemH, has promiscuous activity with this abundant, bioavailable Co^{2+} and produces CoPPIX. When a hemoprotein is contemporaneously overproduced, the CoPPIX is loaded into these proteins as a non-natural cofactor, lessening the toxic effects of both CoPPIX and Co^{2+}.[16] Free metallocofactors may be subject to degradation by heme catabolic pathways, to which the iron cofactor is most susceptible. The net result is efficient heterologous expression of metal-substituted hemoproteins with the CoPPIX cofactor.

The biosynthesis and incorporation of artificial cofactors is a long-standing and alluring challenge in the fields of synthetic biology and biocatalysis. New-to-nature cofactors may imbue enzymes with alternate modes of reactivity, but because these enzymes are difficult and tedious to produce, explorations of their potential activities are rare. The enantioselective carbene and nitrene transfer reactivity of metal-substituted hemoproteins, in particular, has led to the development of several strategies for the incorporation of pre-fabricated metalloporphyrins into hemoproteins.[69] The production of these artificial metalloenzymes remains less efficient than that of the native hemoprotein. This report has described a fully biosynthetic and efficient method for the production and incorporation of the artificial cofactor CoPPIX into hemoproteins. This method operates in rich media and thus enables further development of these proteins as potential biocatalysts.

AUTHOR INFORMATION

Corresponding Author

* Andrew R. Buller – Department of Chemistry, University of Wisconsin-Madison, Madison, Wisconsin 53706, United States; orcid.org/0000-0002-9635-4844; Email: arbuller@wisc.edu.

* Judith N. Burstyn – Department of Chemistry, University of Wisconsin-Madison, Madison, Wisconsin 53706, United States; orcid.org/0000-0003-3245-5563; Email: burstyn@chem.wisc.edu

Author Contribution

L.J.P., B.R.W, F.O.F.C. conducted experiments and collected data. L.J.P, B.R.W, J.N.B., and A.R.B analyzed and interpreted results and prepared the manuscript.

Conflict of interest

The authors declare no competing financial interest.

Funding Sources

This work was supported by the Office of the Vice Chancellor for Research and Graduate Education at the University of Wisconsin-Madison with funding from the Wisconsin Alumni Research Foundation and an NSF CAREER award to A.R.B.

ACKNOWLEDGMENTS

We thank members of the Brunold, Buller, and Burstyn groups for fruitful discussions of this research.

ASSOCIATED CONTENT

Supporting Information. Detailed experimental procedures, protein and DNA sequences, LC/MS spectra, and supporting figures and methods (pdf). This material is available free of charge via the Internet at http://pubs.acs.org.

ABBREVIATIONS

PPIX: Protoporphyrin IX

CoPPIX: cobalt protopophryin IX

*Ec*HemH: *E. coli* ferrochelatase

DyP: Dye Decolorizing Peroxidase

SUMS: substrate multiplexed screening

REFERENCES

(1) Schwizer, F.; Okamoto, Y.; Heinisch, T.; Gu, Y.; Pellizzoni, M. M.; Lebrun, V.; Reuter, R.; Köhler, V.; Lewis, J. C.; Ward, T. R. Artificial Metalloenzymes: Reaction Scope and Optimization Strategies. *Chemical Reviews*. American Chemical Society January 2018, pp 142–231. https://doi.org/10.1021/acs.chemrev.7b00014.

(2) Hartwig, J. F.; Ward, T. R. New "Cats" in the House: Chemistry Meets Biology in Artificial Metalloenzymes and Repurposed Metalloenzymes. *Acc. Chem. Res.* **2019**. https://doi.org/10.1021/ACS.ACCOUNTS.9B00154.

(3) Sreenilayam, G.; Moore, E. J.; Steck, V.; Fasan, R. Metal Substitution Modulates the Reactivity and Extends the Reaction Scope of Myoglobin Carbene Transfer Catalysts. *Adv Synth Catal* **2017**, *359* (12), 2076–2089. https://doi.org/10.1002/adsc.201700202.

(4) Key, H. M.; Dydio, P.; Clark, D. S.; Hartwig, J. F. Abiological Catalysis by Artificial Haem Proteins Containing Noble Metals in Place of Iron. *Nature* **2016**, *534* (7608), 534–537. https://doi.org/10.1038/nature17968.

(5) Brandenberg, O. F.; Fasan, R.; Arnold, F. H. Exploiting and Engineering Hemoproteins for Abiological Carbene and Nitrene Transfer Reactions. *Curr Opin Biotechnol* **2017**, *47*, 102–111. https://doi.org/10.1016/j.copbio.2017.06.005.

(6) Krajewski, A. E.; Lee, J. K. Nucleophilicity and Electrophilicity in the Gas Phase: Silane Hydricity. *J. Org. Chem.* **2022**, *87* (3), 1840–1849. https://doi.org/10.1021/acs.joc.1c02763.

(7) Mondal, A.; Das, M.; Mazumdar, S. Substitution of Iron with Cobalt in the Prosthetic Group of Bacterial Cytochrome P450: Effects on the Stability and Structure of the Protein. *Inorganica Chim. Acta* **2019**, *487* (August 2018), 398–404. https://doi.org/10.1016/j.ica.2018.12.043.

(8) Keita Omura, Yuichiro Aiba*, Kazuto Suzuki, Shinya Ariyasu, Hiroshi Sugimoto, and O. S. A P450 Harboring Manganese Protoporphyrin IX Generates a Manganese Analogue of Compound I by Activating Dioxygen. *ACS Catal.* **2022**, *12* (18), 11108–11117.

(9) Hoffman, B. M.; Petering, D. H. Coboglobins: Oxygen-Carrying Cobalt-Reconstituted Hemoglobin and Myoglobin. *Proc. Natl. Acad. Sci.* **1970**, *67* (2), 637–643. https://doi.org/10.1073/pnas.67.2.637.

(10) Wagner, G. C.; Gunsalus, I. C.; Wang, M.-Y. R.; Hoffman, B. M. Cobalt-Substituted Cytochrome P-450$_{Cam}$. *J. Biol. Chem.* **1981**, *256* (12), 6266–6273.

(11) Wang, M.-Y. R.; Hoffman, B. M.; Hollenberg, P. F. Cobalt-Substituted Horseradish Peroxidase*. *J. Biol. Chem.* **1977**, *252* (18), 6268–6275.

(12) Bruha, A.; Kincaid, J. R. Resonance Raman Studies of Dioxygen Adducts of Co-Substituted Heme Proteins and Model Compounds. Vibrationally Coupled Dioxygen and the Issue of Multiple Structures and Distal Side Hydrogen Bonding. *J. Am. Chem. Soc.* **1988**, *110* (18), 6006–60014.

(13) Woodward, J. J.; Martin, N. I.; Marletta, M. A. An Escherichia Coli Expression-Based Method for Heme Substitution. *Nat. Methods* **2007**, *4* (1), 43–45. https://doi.org/10.1038/nmeth984.

(14) Bordeaux, M.; Singh, R.; Fasan, R. Intramolecular C(Sp3)H Amination of Arylsulfonyl Azides with Engineered and Artificial Myoglobin-Based Catalysts. *Bioorganic Med. Chem.* **2014**, *22* (20), 5697–5704. https://doi.org/10.1016/j.bmc.2014.05.015.

(15) Liu, Z.; Huang, J.; Gu, Y.; Clark, D. S.; Mukhopadhyay, A.; Keasling, J. D.; Hartwig, J. F. Assembly and Evolution of Artificial Metalloenzymes within E. Coli Nissle 1917 for Enantioselective and Site-Selective Functionalization of C—H and C═C Bonds. *J. Am. Chem. Soc.* **2022**, *144* (2), 883–890. https://doi.org/10.1021/jacs.1c10975.

(16) Perkins, L. J.; Weaver, B. R.; Buller, A. R.; Burstyn, J. N. De Novo Biosynthesis of a Nonnatural Cobalt Porphyrin Cofactor in E. Coli and Incorporation into Hemoproteins. *Proc. Natl. Acad. Sci.* **2021**, *118* (16), 2021. https://doi.org/10.1073/PNAS.2017625118.

(17) Labbé, R. F.; Vreman, H. J.; Stevenson, D. K. Zinc

Protoporphyrin: A Metabolite with a Mission. *Clin. Chem.* **1999**, *45* (12), 2060–2072. https://doi.org/10.1093/clinchem/45.12.2060.

(18) Majtan, T.; Frerman, F. E.; Kraus, J. P. Effect of Cobalt on Escherichia Coli Metabolism and Metalloporphyrin Formation. *BioMetals* **2011**, *24* (2), 335–347. https://doi.org/10.1007/s10534-010-9400-7.

(19) Majtan, T.; Freeman, K. M.; Smith, A. T.; Burstyn, J. N.; Kraus, J. P. Purification and Characterization of Cystathionine β-Synthase Bearing a Cobalt Protoporphyrin. *Arch. Biochem. Biophys.* **2011**, *508* (1), 25–30. https://doi.org/10.1016/J.ABB.2011.01.012.

(20) Choi, K. R.; Yu, H. E.; Lee, S. Y. Production of Zinc Protoporphyrin IX by Metabolically Engineered Escherichia Coli. *Biotechnol. Bioeng.* **2022**, *119* (11), 3319–3325. https://doi.org/10.1002/bit.28195.

(21) Jumper, J.; Evans, R.; Pritzel, A.; Green, T.; Figurnov, M.; Ronneberger, O.; Tunyasuvunakool, K.; Bates, R.; Žídek, A.; Potapenko, A.; Bridgland, A.; Meyer, C.; Kohl, S. A. A.; Ballard, A. J.; Cowie, A.; Romera-Paredes, B.; Nikolov, S.; Jain, R.; Adler, J.; Back, T.; Petersen, S.; Reiman, D.; Clancy, E.; Zielinski, M.; Steinegger, M.; Pacholska, M.; Berghammer, T.; Bodenstein, S.; Silver, D.; Vinyals, O.; Senior, A. W.; Kavukcuoglu, K.; Kohli, P.; Hassabis, D. Highly Accurate Protein Structure Prediction with AlphaFold. *Nat. 2021 5967873* **2021**, *596* (7873), 583–589. https://doi.org/10.1038/s41586-021-03819-2.

(22) Bryant, D. A.; Hunter, C. N.; Warren, M. J. Biosynthesis of the Modified Tetrapyrroles—the Pigments of Life. *J. Biol. Chem.* **2020**, *295* (20), 6888–6925. https://doi.org/10.1074/JBC.REV120.006194.

(23) Medlock, A.; Swartz, L.; Dailey, T. A.; Dailey, H. A.; Lanzilotta, W. N. Substrate Interactions with Human Ferrochelatase. *Proc. Natl. Acad. Sci. U. S. A.* **2007**, *104* (6), 1789–1793. https://doi.org/10.1073/pnas.0606144104.

(24) Gora, M.; Grzybowska, E.; Rytka, J.; Labbe-Bois, R. Probing the Active-Site Residues in Saccharomyces Cerevisiae Ferrochelatase by Directed Mutagenesis. *J. Biol. Chem.* **1996**, *271* (20), 11810–11816. https://doi.org/10.1074/jbc.271.20.11810.

(25) Dailey, H. A.; Dailey, T. A.; Wu, C. K.; Medlock, A. E.; Rose, J. P.; Wang, K. F. Ferrochelatase at the Millennium: Structures, Mechanisms and [2Fe-2S] Clusters. *Cell. Mol. Life Sci.* **2000**, *57* (13–14), 1909–1926. https://doi.org/10.1007/PL00000672.

(26) Sudhamsu, J.; Kabir, M.; Airola, M. V; Patel, B. A.; Yeh, S. R.; Rousseau, D. L.; Crane, B. R. Co-Expression of Ferrochelatase Allows for Complete Heme Incorporation into Recombinant Proteins Produced in E. Coli. *Protein Expr Purif* **2010**, *73* (1), 78–82. https://doi.org/10.1016/j.pep.2010.03.010.

(27) Miyamoto, K.; Kanaya, S.; Morikawa, K.; Inokuchi, H. Overproduction, Purification, and Characterization of Ferrochelatase from Escherichia Coli1. *J. Biochem.* **1994**, *115* (3), 545–551. https://doi.org/10.1093/oxfordjournals.jbchem.a124373.

(28) Hunter, G. A.; Ferreira, G. C. Metal Ion Coordination Sites in Ferrochelatase. *Coord. Chem. Rev.* **2022**, *460*, 214464. https://doi.org/10.1016/j.ccr.2022.214464.

(29) Kohno, H.; Okuda, M.; Furukawa, T.; Tokunaga, R.; Taketani, S. Site-Directed Mutagenesis of Human Ferrochelatase: Identification of Histidine-263 as a Binding Site for Metal Ions. *Biochim. Biophys. Acta (BBA)/Protein Struct. Mol.* **1994**, *1209* (1), 95–100. https://doi.org/10.1016/0167-4838(94)90142-2.

(30) Davidson, R. E.; Chesters, C. J.; Reid, J. D. Metal Ion Selectivity and Substrate Inhibition in the Metal Ion Chelation Catalyzed by Human Ferrochelatase *. *J. Biol. Chem.* **2009**, *284* (49), 33795–33799. https://doi.org/10.1074/JBC.M109.030205.

(31) McIntyre, N. R.; Franco, R.; Shelnutt, J. A.; Ferreira, G. C. Nickel(II) Chelatase Variants Directly Evolved from Murine Ferrochelatase: Porphyrin Distortion and Kinetic Mechanism. *Biochemistry* **2011**, *50* (9), 1535–1544. https://doi.org/10.1021/bi101170p.

(32) Hunter, G. A.; Sampson, M. P.; Ferreira, G. C. Metal Ion Substrate Inhibition of Ferrochelatase. *J. Biol. Chem.* **2008**, *283* (35), 23685–23691. https://doi.org/10.1074/jbc.M803372200.

(33) Al-Karadaghi, S.; Franco, R.; Hansson, M.; Shelnutt, J. A.; Isaya, G.; Ferreira, G. C. Chelatases: Distort to Select? *Trends Biochem. Sci.* **2006**, *31* (3), 135–142. https://doi.org/10.1016/J.TIBS.2006.01.001.

(34) Blackwood, M. E.; Rush, T. S.; Romesberg, F.; Schultz, P. G.; Spiro, T. G. Alternative Modes of Substrate Distortion in Enzyme and Antibody Catalyzed Ferrochelation Reactions. *Biochemistry* **1998**, *37* (3), 779–782. https://doi.org/10.1021/bi972616f.

(35) Franco, R.; Ma, J.-G.; Lu, Y.; Ferreira, G. C.; Shelnutt, J. A. Porphyrin Interactions with Wild-Type and Mutant Mouse Ferrochelatase. *Biochemistry* **2000**, *39* (10), 2517–2529. https://doi.org/10.1021/bi991346t.

(36) Medlock, A. E.; Najahi-Missaoui, W.; Shiferaw, M. T.; Albetel, A. N.; Lanzilotta, W. N.; Dailey, H. A. Insight into the Function of Active Site Residues in the Catalytic Mechanism of Human Ferrochelatase. **2021**. https://doi.org/10.1042/BCJ20210460.

(37) Gillam, M. E.; Hunter, G. A.; Ferreira, G. C. Ferrochelatase π-Helix: Implications from Examining the Role of the Conserved π-Helix Glutamates in Porphyrin Metalation and Product Release. *Arch. Biochem. Biophys.* **2018**, *644*, 37–46. https://doi.org/10.1016/j.abb.2018.02.015.

(38) Medlock, A. E.; Carter, M.; Dailey, T. A.; Dailey, H. A.; Lanzilotta, W. N. Product Release Rather than Chelation Determines Metal Specificity for Ferrochelatase. *J. Mol. Biol.* **2009**, *393* (2), 308–319. https://doi.org/10.1016/j.jmb.2009.08.042.

(39) Medlock, A. E.; Najahi-Missaoui, W.; Shiferaw, M. T.; Albetel, A. N.; Lanzilotta, W. N.; Dailey, H. A. Insight into the Function of Active Site Residues in the Catalytic Mechanism of Human Ferrochelatase. *Biochem. J.* **2021**, *478* (17), 3239–3252. https://doi.org/10.1042/BCJ20210460.

(40) Sellers, V. M.; Wu, C. K.; Dailey, T. A.; Dailey, H. A. Human Ferrochelatase: Characterization of Substrate - Iron Binding and Proton-Abstracting Residues. *Biochemistry* **2001**, *40* (33), 9821–9827. https://doi.org/10.1021/BI010012C/ASSET/IMAGES/LARGE/BI010012CF00006.JPEG.

(41) Brindley, A. A.; Raux, E.; Leech, H. K.; Schubert, H. L.; Warren, M. J. A Story of Chelatase Evolution: Identification and Characterization of a Small 13-15-KDa "Ancestral" Cobaltochelatase (CbiXs) in the Archaea. *J. Biol. Chem.* **2003**, *278* (25), 22388–22395. https://doi.org/10.1074/jbc.M302468200.

(42) Dailey, H. A.; Dailey, T. A.; Wu, C.-K.; Medlock, A. E.; Rose, J. P.; Wang, K.-F. Ferrochelatase at the Millennium: Structures, Mechanisms and [2Fe-2S] Clusters. *Cell. Mol. Life Sci.* **2000**, *57* (13), 1909–1926. https://doi.org/10.1007/PL00000672.

(43) Gates, C. A.; Northrop, D. B. Kinetic Distinction between Rapid-Equilibrium Random and Abortive Ordered Enzymatic Mechanisms Using Alternative Substrates or Kinetic Isotope Effects. *Biochem. Biophys. Res. Commun.* **1988**, *152* (1), 406–410. https://doi.org/10.1016/S0006-291X(88)80728-9.

(44) Crooks, G. E.; Hon, G.; Chandonia, J.-M.; Brenner, S. E. WebLogo: A Sequence Logo Generator: Figure 1. *Genome Res.* **2004**, *14* (6), 1188–1190. https://doi.org/10.1101/gr.849004.

(45) Arnold, F. H. Design by Directed Evolution. *Acc. Chem. Res.* **1998**, *31* (3), 125–131. https://doi.org/10.1021/ar960017f.

(46) Herger, M.; Van Roye, P.; Romney, D. K.; Brinkmann-Chen, S.; Buller, A. R.; Arnold, F. H. Synthesis of β-Branched Tryptophan Analogues Using an Engineered Subunit of Tryptophan Synthase. *J. Am. Chem. Soc.* **2016**, *138* (27), 8388–8391. https://doi.org/10.1021/jacs.6b04836.

(47) Ellis, J. M.; Campbell, M. E.; Kumar, P.; Geunes, E. P.; Bingman, C. A.; Buller, A. R. Biocatalytic Synthesis of Non-Standard Amino Acids by a Decarboxylative Aldol Reaction. *Nat. Catal.* **2022**, *5* (2), 136–143. https://doi.org/10.1038/s41929-022-00743-0.

(48) Weeks, A. M.; Wells, J. A. Engineering Peptide Ligase Specificity by Proteomic Identification of Ligation Sites. *Nat. Chem. Biol.* **2018**, *14* (1), 50–

57. https://doi.org/10.1038/nchembio.2521.

(49) Mcdonald, A. D.; Higgins, P. M.; Buller, A. R. Substrate Multiplexed Protein Engineering Facilitates Promiscuous Biocatalytic Synthesis. 2021. https://doi.org/10.26434/CHEMRXIV-2021-XL252.

(50) McDonald, A. D.; Bruffy, S. K.; Kasat, A. T.; Buller, A. R. Engineering Enzyme Substrate Scope Complementarity for Promiscuous Cascade Synthesis of 1,2-Amino Alcohols. *Angew. Chemie Int. Ed.* 2022, *61* (46), e202212637. https://doi.org/10.1002/ANIE.202212637.

(51) Sellers, V. M.; Wu, C.-K.; Dailey, T. A.; Dailey, H. A. Human Ferrochelatase: Characterization of Substrate−Iron Binding and Proton-Abstracting Residues. *Biochemistry* 2001, *40* (33), 9821–9827. https://doi.org/10.1021/bi010012c.

(52) Medlock, A. E.; Dailey, T. A.; Ross, T. A.; Dailey, H. A.; Lanzilotta, W. N. A π-Helix Switch Selective for Porphyrin Deprotonation and Product Release in Human Ferrochelatase. *J. Mol. Biol.* 2007, *373* (4), 1006–1016. https://doi.org/10.1016/j.jmb.2007.08.040.

(53) Colpa, D. I.; Fraaije, M. W. High Overexpression of Dye Decolorizing Peroxidase TfuDyP Leads to the Incorporation of Heme Precursor Protoporphyrin IX. *J. Mol. Catal. B Enzym.* 2016, *134*, 372–377. https://doi.org/10.1016/j.molcatb.2016.08.017.

(54) Hunter, G. A.; Ferreira, G. C. Molecular Enzymology of 5-Aminolevulinate Synthase, the Gatekeeper of Heme Biosynthesis. *Biochim. Biophys. Acta* 2011, *1814* (11), 1467–1473. https://doi.org/10.1016/j.bbapap.2010.12.015.

(55) Woodard, S. I.; Dailey, H. A. Regulation of Heme Biosynthesis in Escherichia Coli. *Arch. Biochem. Biophys.* 1995, *316* (1), 110–115. https://doi.org/10.1006/ABBI.1995.1016.

(56) McNicholas, P. M.; Javor, G.; Darie, S.; Gunsalus, R. P. Expression of the Heme Biosynthetic Pathway Genes HemCD, HemH, HemM and HemA of Escherichia Coli. *FEMS Microbiol. Lett.* 2006, *146* (1), 143–148. https://doi.org/10.1111/j.1574-6968.1997.tb10184.x.

(57) Foster, A. W.; Clough, S. E.; Aki, Z.; Young, T. R.; Clarke, A. R.; Robinson, N. J. Metalation Calculators for E. Coli Strain JM109 (DE3): Aerobic, Anaerobic, and Hydrogen Peroxide Exposed Cells Cultured in LB Media. *Metallomics* 2022, *14* (9). https://doi.org/10.1093/mtomcs/mfac058.

(58) Wu, J.; Wen, S.; Zhou, Y.; Chao, H.; Shen, Y. Human Ferrochelatase: Insights for the Mechanism of Ferrous Iron Approaching Protoporphyrin IX by QM/MM and QTCP Free Energy Studies. *J. Chem. Inf. Model.* 2016, *56* (12), 2421–2433. https://doi.org/10.1021/acs.jcim.6b00216.

(59) Studier, F. W.; Daegelen, P.; Lenski, R. E.; Maslov, S.; Kim, J. F. Understanding the Differences between Genome Sequences of Escherichia Coli B Strains REL606 and BL21(DE3) and Comparison of the E. Coli B and K-12 Genomes. *J. Mol. Biol.* 2009, *394* (4), 653–680. https://doi.org/10.1016/j.jmb.2009.09.021.

(60) Rodrigue, A.; Effantin, G.; Mandrand-Berthelot, M.-A. Identification of RcnA (YohM), A Nickel and Cobalt Resistance Gene in Escherichia Coli. *J. Bacteriol.* 2005, *187* (8), 2912–2916.

(61) Blériot, C.; Effantin, G.; Lagarde, F.; Mandrand-Berthelot, M.-A.; Rodrigue, A. RcnB Is a Periplasmic Protein Essential for Maintaining Intracellular Ni and Co Concentrations in Escherichia Coli. *J. Bacteriol.* 2011, *193* (15), 3785–3793. https://doi.org/10.1128/JB.05032-11.

(62) Phue, J. N.; Kedem, B.; Jaluria, P.; Shiloach, J. Evaluating Microarrays Using a Semiparametric Approach: Application to the Central Carbon Metabolism of Escherichia Coli BL21 and JM109. *Genomics* 2007, *89* (2), 300–305. https://doi.org/10.1016/j.ygeno.2006.10.004.

(63) Suits, M. D. L.; Jaffer, N.; Jia, Z. Structure of the Escherichia Coli O157:H7 Heme Oxygenase ChuS in Complex with Heme and Enzymatic Inactivation by Mutation of the Heme Coordinating Residue His-193. *J. Biol. Chem.* 2006, *281* (48), 36776–36782. https://doi.org/10.1074/jbc.M607684200.

(64) Suits, M. D. L.; Pal, G. P.; Nakatsu, K.; Matte, A.; Cygler, M.; Jia, Z. Identification of an Escherichia

Coli O157:H7 Heme Oxygenase with Tandem Functional Repeats. *Proc. Natl. Acad. Sci.* **2005**, *102* (47), 16955–16960. https://doi.org/10.1073/pnas.0504289102.

(65) Yoshinaga, T.; Sassa, S.; Kappas, A. Purification and Properties of Bovine Spleen Heme Oxygenase. Amino Acid Composition and Sites of Action of Inhibitors of Heme Oxidation. *J. Biol. Chem.* **1982**, *257* (13), 7778–7785. https://doi.org/10.1016/S0021-9258(18)34449-1.

(66) Lee, W. C.; Reniere, M. L.; Skaar, E. P.; Murphy, M. E. P. Ruffling of Metalloporphyrins Bound to IsdG and IsdI, Two Heme-Degrading Enzymes in Staphylococcus Aureus. *J. Biol. Chem.* **2008**, *283* (45), 30957–30963. https://doi.org/10.1074/jbc.M709486200.

(67) Létoffé, S.; Heuck, G.; Delepelaire, P.; Lange, N.; Wandersman, C. Bacteria Capture Iron from Heme by Keeping Tetrapyrrol Skeleton Intact. *Proc. Natl. Acad. Sci. U. S. A.* **2009**, *106* (28), 11719–11724. https://doi.org/10.1073/PNAS.0903842106/SUPPL_FILE/0903842106SI.PDF.

(68) Dailey, H. A.; Septer, A. N.; Daugherty, L.; Thames, D.; Gerdes, S.; Stabb, E. V.; Dunn, A. K.; Dailey, T. A.; Phillips, J. D. The Escherichia Coli Protein YfeX Functions as a Porphyrinogen Oxidase, Not a Heme Dechelatase. *MBio* **2011**, *2* (6). https://doi.org/10.1128/MBIO.00248-11.

(69) Bloomer, B. J.; Clark, D. S.; Hartwig, J. F. Progress, Challenges, and Opportunities with Artificial Metalloenzymes in Biosynthesis. *Biochemistry* **2023**, *62* (2), 221–228. https://doi.org/10.1021/acs.biochem.1c00829.

For table of contents use only:

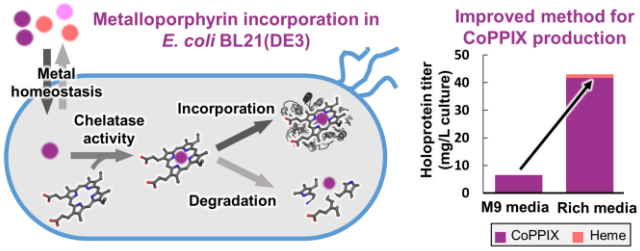

Title: Molecular determinates of efficient cobalt-substituted hemoprotein production in E. coli

Authors: Brian R. Weaver, Lydia J. Perkins, Froylan Omar Fernandez Candelaria, Judith N. Burstyn, Andrew R. Buller